Light emission efficiency and imaging performance of $Gd_2O_2S:Eu$ powder scintillator under x-ray radiography conditions

C. M. Michail
Department of Medical Physics, Faculty of Medicine, University of Patras, 265 00 Patras, Greece

G. P. Fountos, P. F. Liaparinos, N. E. Kalyvas, I. Valais, and I. S. Kandarakis[a)]
Department of Medical Instruments Technology, Technological Educational Institute, 122 10 Athens, Greece

G. S. Panayiotakis
Department of Medical Physics, Faculty of Medicine, University of Patras, 265 00 Patras, Greece

(Received 22 December 2009; revised 26 March 2010; accepted for publication 14 May 2010; published 24 June 2010)

Purpose: To evaluate $Gd_2O_2S:Eu$ powder phosphor as a radiographic image receptor and to compare it to phosphors often used in radiography. $Gd_2O_2S:Eu$ is nonhygroscopic, emitting red light with decay time close to that of $Gd_2O_2S:Tb$.
Methods: The light intensity emitted per unit of x-ray exposure rate (absolute luminescence efficiency) was measured for laboratory prepared screens with coating thicknesses of 33.1, 46.4, 63.1, 78.3, and 139.8 mg/cm^2 and tube voltages ranging from 50 to 140 kVp. Parameters related to image quality such as the modulation transfer function (MTF) and the detective quantum efficiency (DQE) were also experimentally examined. In addition, a previously validated Monte Carlo code was used to estimate intrinsic x-ray absorption and optical properties, as well as the MTF and the Swank factor (I) of the $Gd_2O_2S:Eu$ scintillators.
Results: $Gd_2O_2S:Eu$ light intensity was found higher than that of single CsI:Tl crystal for tube voltages up to 100 kVp. The MTF and the DQE were found to be comparable with those of $Gd_2O_2S:Tb$ and CsI:Tl screens. MTF estimated by the Monte Carlo code was found very close to the experimental MTF values. $Gd_2O_2S:Eu$ showed peak emission in the wavelength range 620–630 nm. Its emission spectrum was excellently matched to various optical detectors (photodiodes, photocathodes, CCDs, and CMOS) employed in flat panel detectors.
Conclusions: $Gd_2O_2S:Eu$ is an efficient phosphor potentially well suited to radiography and especially to some digital detectors sensitive to red light. © *2010 American Association of Physicists in Medicine*. [DOI: 10.1118/1.3451113]

Key words: radiation detectors, phosphor screens, light emission efficiency, imaging performance, x-ray radiography

I. INTRODUCTION

Most radiation detectors consist of a scintillator (phosphor) screen coupled to an optical detector (photographic emulsion film, photocathode, photodiode, etc.).[1–5] Terbium (Tb)-activated phosphors (i.e., $Gd_2O_2S:Tb$ and, in some cases, $La_2O_2S:Tb$ and $Y_2O_2S:Tb$) have been, up to now, accepted to be one of the most efficient x-ray-to-light converters[1–4] employed in screen-film mammography and radiography. Currently, the most preferred phosphors are $Gd_2O_2S:Tb$ and CsI:Tl. $Gd_2O_2S:Tb$ has been proven very useful in conventional screen-film radiography systems, where adequate matching of the film's spectral sensitivity to the emission of the phosphor, as well as high sensitivity of the film at the particular wavelength range, is of primary consideration in order to obtain the highest speed for the screen-film combination. However, in some digital imaging systems, based on crystalline silicon (Si) optical detectors [charge-coupled devices (CCDs) and photodiodes], the green light emitted by terbium-activated phosphors is not very efficiently detected. This is because a large number of Si and CMOS based devices incorporated in x-ray imaging systems are not adequately sensitive to these wavelengths (500–550 nm); only 45%–55% of the light produced by $Gd_2O_2S:Tb$ or other terbium-activated phosphors is registered by the Si photodiode.[3] Since most Si and CMOS based photodetectors are more sensitive to longer wavelength ranges, and particularly in the red wavelength range, it would be of interest to investigate the emission efficiency of red emitting phosphors.[6–9]

Such phosphors can be easily prepared by inserting europium ion activator (Eu^{3+}) in rare earth based host matrices. Furthermore, many europium doped scintillators, and particularly $Gd_2O_2S:Eu$, have been previously found comparable to terbium-activated phosphors in terms of optical output.[9] In addition, europium-activated phosphors have a decay time of the order of 1 ms (slightly higher than $Gd_2O_2S:Tb$), which is acceptable for applications that do not involve high framing rates.[10,11] These include stationary digital and conventional radiography, i.e., general radiography and mammography. $Gd_2O_2S:Eu$ has been previously employed in single pulse dual energy radiography,[12] in digital mammography, and in diffraction enhanced breast imaging

with CCD arrays.[13–16] In a recent study of our group,[17] data on the $Gd_2O_2S:Eu$ scintillator were reported mainly concerning intrinsic properties such as x-ray absorption, intrinsic x-ray-to-light conversion, emitted spectrum, and spectral compatibility to optical sensors in the mammographic energy range. In the present study, the imaging properties of $Gd_2O_2S:Eu$ scintillator were systematically investigated. This was accomplished by experimental evaluation of various parameters related to image brightness, image resolution, and signal to noise ratio. The scintillator was used in the form of screens (layers) of various thickness and the parameters investigated were the absolute efficiency (AE)[4] and the detector quantum gain (DQG),[17] both expressing the light emission efficiency of the scintillator, the spectral compatibility to optical detectors,[17] the modulation transfer function (MTF), the noise power spectrum (NPS), and the detective quantum efficiency (DQE).[5] In addition, a custom-developed and previously validated Monte Carlo (MC) simulation code,[2] based on the Mie light scattering theory, was used to assess x-ray absorption and optical properties of this phosphor. Furthermore, MTF data were derived by this MC code and were compared to experimental MTF values.[2] Although $Gd_2O_2S:Eu$ is not a new scintillator, its properties have not been previously systematically investigated under x-ray imaging conditions for use in digital detectors.

II. MATERIALS AND METHODS

II.A. Experiments and calculations

$Gd_2O_2S:Eu$ was purchased in powder form (Phosphor Technology Ltd., Stevenage Herts, England, code: UKL63/N-R1) with mean grain size of approximately 8 μm and a density of 7.3 g/cm^3. Grain size affects both resolution and efficiency. However, it is generally accepted that sizes in the range from 5 to 10 μm give a satisfactory compromise between resolution and efficiency.[1,3] The phosphor was studied in the form of thin layers (test screen). For the purposes of the present study, five scintillating screens with coating thicknesses of 33.1, 46.4, 63.1, 78.3, and 139.8 mg/cm^2 were prepared by sedimentation of $Gd_2O_2S:Eu$ powder on fused silica substrate (spectrosil B). Sedimentation has been a widely accepted technique for preparation of radiographic phosphor screens with good homogeneity in various dimensions (i.e., area and thickness) and spatial resolution.[18,19] The screens were obtained with a packing density of the order of 50%, which is common in commercial phosphor screens.[18,19] Other techniques, such as sintering, have been also employed providing ceramic scintillating screens with high packing density and good homogeneity.[20] It was previously estimated that such screens can show improved resolution.[11,21] However, this method is more complex and not well established yet. The optical properties of the fused silica (spectrosil B) substrate have been measured via a Perkin-Elmer (Waltham, MA) Lambda 15 UV/VIS spectrophotometer. In the visible range, the optical transparency was found very high, of the order of 93%, while absorption was found very low (0.029). These values show that the substrate has very high transparency, low reflectivity, and low absorption in the wavelength range of the phosphor emission. During the sedimentation process, sodium orthosilicate (Na_2SiO_3) was used as binding material between the powder grains.[17] Experiments were performed on a Philips Optimus x-ray unit. Tube filtration was 2.5 mm Al. Appropriate beam filtering (21 mm Al) was applied to simulate x-ray beam hardening by the human body.[22] Incident exposure rate measurements were performed using a Wellhöfer dosimeter WD10 (Wellhöfer Dosimetrie, Schwarzenbruck, Germany). Tube voltage was checked using a Victoreen (Fluke Biomedical, Everett, WA) dosimeter Model 4000 M+.

II.A.1. Absolute luminescence efficiency (AE)

The absolute efficiency was determined by measuring the light energy flux emitted by the irradiated screen and dividing by the incident exposure rate measured at screen position. The experimental setup for light energy flux measurements comprised a light integration sphere (Oriel 70451) coupled to a photomultiplier (EMI 9798 B) with an extended sensitivity S-20 photocathode, and was enclosed within a bronze light tight chamber. The sample (screen) is placed in the input port of the integration sphere. The outer surface of this port was covered by a light tight adaptor. The light is diffused on the inner surface of the sphere undergoing multiple reflections, assuring homogenous illumination of the photocathode, which was placed at the output port of the sphere. The light throughput, i.e., fraction of light transmitted through the sphere, can be calculated and it is constant for the same shape of all types of scintillator samples, assuring computable fraction of light losses. The photomultiplier current was amplified and fed to a vibrating reed (Cary 401) electrometer operated in current mode. An analog to digital converter was employed to digitize electrometer's output, which was then stored in a computer. AE was computed from electrometer's output current and dosimeter data by a method already described in literature[22]

$$\mathrm{AE} = \Psi_\Lambda / X = \left[\frac{I_{\mathrm{elec}}}{\tau_0 (s_{\mathrm{PC}} a_s)} \cdot \frac{1}{A_{\mathrm{sc}}} \right] \cdot X^{-1}, \quad (1)$$

where Ψ_Λ is the emitted light energy flux (energy of light per unit of area and time), X is the incident exposure rate that excites the phosphor to luminescence, I_{elec} is the current at the output of the electrometer (in pA), s_{PC} is the peak photosensitivity of the photocathode (in pA/W), which was used as a factor converting the output photocathode current into light energy flux. a_s (see Sec. II A 3) is the spectral matching factor of the screen's emission spectrum to the spectral sensitivity of the photocathode (extended S-20) and A_{sc} is the irradiated area of the screen. τ_0 denotes the throughput of the integration sphere (Oriel 70451 integrating sphere data sheet). AE was finally expressed in units of $\mu W\ m^{-2}/mR\ s^{-1}$, where $\mu W\ m^{-2}$ corresponds to the light energy flux (Ψ_Λ) and $mR\ s^{-1}$ to exposure rate X. For simplicity the notation, efficiency unit (EU) was used (1 EU $= \mu W\ m^{-2}/mR\ s^{-1}$).[22]

II.A.2. Detector quantum gain (DQG)

Detector quantum gain was determined as the ratio

$$\mathrm{DQG} = \Phi_\Lambda / \Phi_X, \tag{2}$$

where Φ_Λ, the emitted light photon fluence, was calculated by $\Psi_\Lambda / hc\bar{\lambda}^{-1}$, where the numerator is the light energy fluence and the denominator is the mean energy E_λ of the emitted light photons ($E_\lambda = hc/\bar{\lambda}$), $\bar{\lambda}$ being the mean light wavelength determined from emission spectra measurements.[17] Φ_X denotes the incident x-ray photon fluence determined from exposure measurements and taking into account the x-ray spectrum according to a method described in the literature (see Appendix B).[23,24]

II.A.3. Optical emission and spectral compatibility to optical detectors

The spectral compatibility between the emitted phosphor light and the spectral sensitivity of various optical detectors (CCDs, photodiodes, CMOS sensors, films, etc.) was calculated by the spectral matching factor (α_S) according to Eq. (3)

$$\alpha_S = \int S_P(\lambda) S_D(\lambda) d\lambda / \int S_P(\lambda) d\lambda, \tag{3}$$

where $S_P(\lambda)$ is the emitted light spectrum of the phosphor and $S_D(\lambda)$ is the spectral sensitivity of the optical detector coupled to the phosphor.[25] The $S_P(\lambda)$ of the $Gd_2O_2S:Eu$ powder phosphor screens was measured under x-ray excitation by an optical spectrometer (Ocean Optics Inc., Dunedin, FL, HR2000).

II.A.4. Modulation transfer function (MTF)

MTF was experimentally determined by the square wave response function (SWRF) method.[26,27] A Nuclear Associates resolution test pattern (typ-53, Nuclear Associates, Fluke Biomedical, Everett, WA) containing Pb lines of various widths corresponding to various spatial frequencies (from 0.25 to 10 lp mm^{-1}) was used to obtain pattern images. The screen was brought in close contact with a radiographic film (Agfa LT 2B) enclosed in a light tight cassette. MTF was measured in transmission mode, i.e., (front screen configuration) where the light from the nonirradiated screen side was measured. The film-screen combination was irradiated by x rays on the radiographic unit. The exposure conditions employed for the MTF measurements were 74 kV at an exposure level corresponding to 0.27 mGy entrance air kerma at the screen surface, at a SDD of 140 cm. After irradiation, films were developed in an Agfa Classic EOS film processor, operated at 35 °C and at 60 s processing time. Pattern images, obtained on the films, were digitized in an Agfa Duoscan scanner with scanning parameters 1000 dpi, 8 bit. Prior to digitization, it was verified that the film optical density values were within the linear part of the H&D characteristic curve. However, screen-film nonlinearities were corrected via the H&D characteristic curve determined using the bootstrap sensitometry technique.[26,28] MTFs were finally calculated from the digitized image optical density variations (digital SWRF). The latter were obtained across directions vertical with respect to the test pattern lines, employing Coltman's formula, which gives the MTF as a function of SWRF.[26,29] The MTF data, obtained in this way, were corrected by dividing by the MTF of the scanner and the MTF of the film, both measured in a previous study.[30]

II.A.5. Noise power spectrum (NPS)

The NPS was experimentally obtained by fast Fourier transforming the optical density fluctuations on six ROIs of 128×128 pixels for each screen.[31,32] The calculated NPS_T contained the noise components of the radiographic film and the scanner. The corresponding components were found by illuminating the film with ambient light until the same optical density with the irradiated film was obtained. The film was subsequently scanned. The NPS_f of the scanned film was subtracted from NPS_T. The resulting NPS corresponds to screen noise (quantum and screen structure noise).[31,33–36] For NPS determination, the x-ray exposure was 0.27 mGy. NPS was also corrected for screen-film nonlinearities via the H&D characteristic curve.[26] Normalized NPS was calculated by dividing NPS by the gain[37] of the screen, according to the relation

$$\mathrm{NNPS}(f) = \mathrm{NPS}(f) / (\mathrm{DQG} \cdot \Phi_X)^2. \tag{4}$$

II.A.6. Detective quantum efficiency (DQE)

The detective quantum efficiency of a scintillating screen expresses the output over the input signal to noise ratio squared.[38,39] In the spatial frequency domain, DQE may be written as follows:[8]

$$\mathrm{DQE}(f) = \frac{(\Phi_\Lambda(E_0)\mathrm{MTF}(f))^2}{\mathrm{NPS}(f)\mathrm{SNR}_{\mathrm{in}}^2}, \tag{5}$$

where $\mathrm{SNR}_{\mathrm{in}}^2$ is the input signal to noise ratio, which can be determined from exposure measurements (see Appendix B). Since the spatial frequency sampling steps of MTF and NPS are generally not the same, NPS was linearly interpolated at the frequency sampling points of MTF and then DQE was calculated at these points.

II.B. Monte Carlo simulation

The MC model used in the present work was developed in previous studies[2] and uses only physical (complex refractive index and light wavelength) and structural (grain size and packing density) characteristics of the phosphor as input data. The simulation code was based on (a) the basic x-ray interactions within the phosphor mass and (b) the light interactions described by the Mie scattering algorithm.[2]

II.B.1. Quantum detection and energy absorption efficiency (QDE and EAE)

The efficiency of a scintillator to detect photons is conventionally described by the quantum detection efficiency (QDE), which is defined as the fraction of incident photons

interacting with the scintillator mass.[23] However, accurate x-ray detection may be determined by considering only those x-ray photons that deposit an amount of energy in the phosphor mass. This is because only these x-rays can generate (scintillations) light signals which may then be detected by the optical sensor and contribute to image formation. The fraction of energy depositing photons is expressed through the energy absorption efficiency (EAE). QDE as well as EAE were also evaluated analytically,[23] as described in previous studies.[17] The required values for the total attenuation and the total energy absorption coefficients of $Gd_2O_2S:Eu$ scintillator were calculated from tabulated data on energy absorption and attenuation coefficients of gadolinium, sulfur, and oxygen.[40,41]

II.B.2. Modulation transfer function (MTF)

After x-ray energy deposition within the phosphor screen, an amount of light photons is produced.[42,43] Light is emitted following an isotropic distribution, according to Mie scattering theory, its propagation within the screen can be expressed by the light extinction coefficient m_{ext}, which is computed by the following formula:[43]

$$m_{\text{ext}} = V_d A Q_{\text{ext}}, \tag{6}$$

where V_d is the volume density of the phosphor screen and A is the geometrical cross-section of the grain and Q_{ext} the extinction efficiency factor. The direction of light photon was simulated according to the Henyey–Greenstein[2] distribution and the anisotropy factor g (depending on physical and structural properties of the phosphor screen) was calculated using the following equation:

$$g = \int_0^{\pi} 2\pi S_{11}(\theta)\cos\,\theta \sin\,\theta d\theta \left[\int_0^{\pi} 2\pi S_{11}(\theta)\sin\,\theta d\theta\right]^{-1}, \tag{7}$$

where $S_{11}(\theta)$ is the first element of the so-called Mueller matrix.[2] To predict the MTF of a phosphor screen by our Monte Carlo simulation model, pencil beam geometry was employed. To evaluate MTF, a two-dimensional point spread function is first obtained using the optical photon distribution on the emitting surface of the screen. Then, a fast Fourier transform is applied on the one-dimensional line spread function, normalizing its value to unity at zero spatial frequency.[2]

II.B.3. Zero-frequency DQE and Swank factor

The Swank factor (I) arises from the fluctuations in the number m of light photons emitted from the screen surface per absorbed x-ray photon and it is defined as[43]

$$I = M_1^2/(M_0 M_2), \tag{8}$$

where M_n is the nth moment of the light pulse height statistical distribution (statistical distribution of values of m).[43] This statistical distribution expresses the fluctuations in the number of light photons emitted by the screen per detected x-ray photon. Taking into account the Swank factor as well as the QDE of the screen, the zero-frequency DQE of the screen can be estimated. DQE, associated with the overall signal to noise transfer properties of the system, may be as given below[43]

$$\text{DQE} = \text{QDE} \cdot I. \tag{9}$$

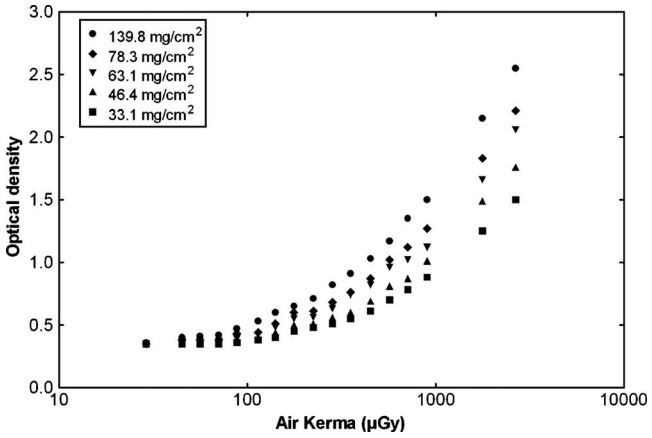

FIG. 1. Density curves of the $Gd_2O_2S:Eu$ Agfa LT 2B screen-film combinations.

III. RESULTS AND DISCUSSION

Figure 1 shows the H&D characteristic curves for the $Gd_2O_2S:Eu$ screens combined with the Agfa LT 2B film. These curves have been used to convert optical density data into air kerma values in the process of MTF and NPS evaluation. In Figs. 2 and 3, QDE and EAE Monte Carlo values were compared to values obtained analytically for x-ray detection. Values of QDE found by Monte Carlo were always slightly lower due to the fraction of incident x rays undergoing elastic scattering events and escaping the converter with no energy deposition (e.g., $\text{QDE}_{\text{MC}}=0.30$ and $\text{QDE}_{\text{analytical}}=0.31$ for the 46.4 mg/cm^2 at 70 kVp in Fig. 3). However,

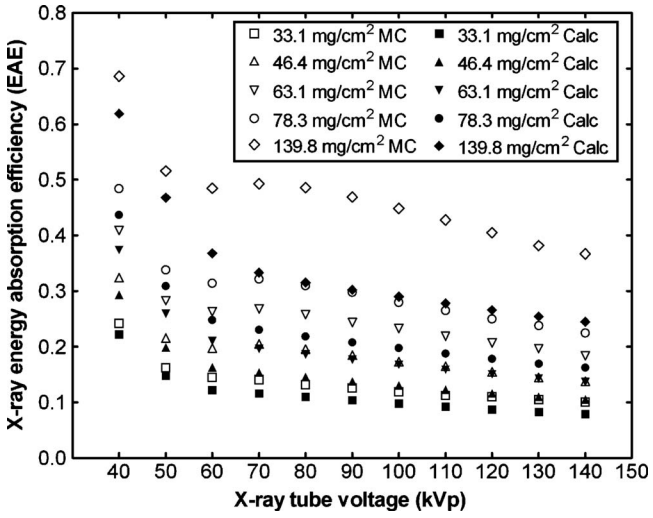

FIG. 2. X-ray EAE comparison between MC and analytical calculations for the $Gd_2O_2S:Eu$ screens in the radiographic energy range.

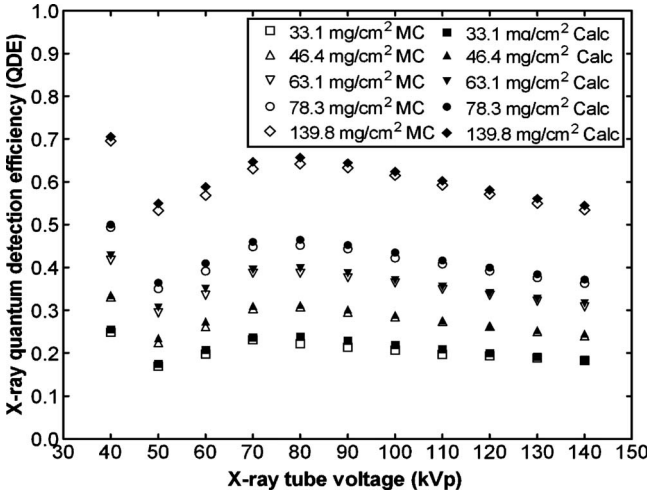

FIG. 3. X-ray QDE comparison between MC and analytical calculations for the Gd_2O_2S:Eu screens in the radiographic energy range.

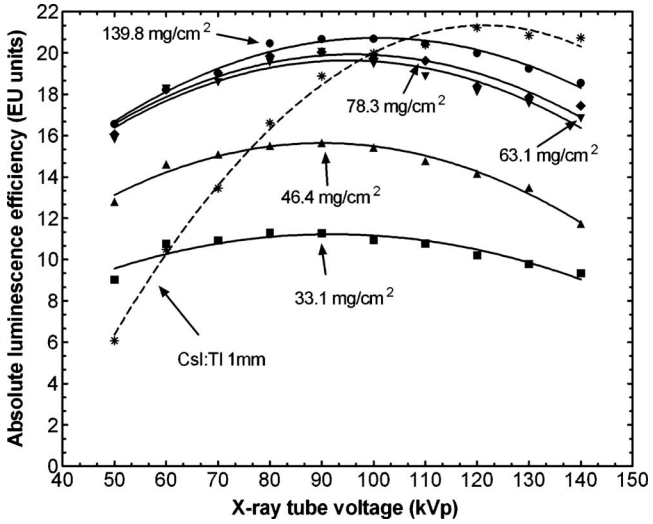

FIG. 4. Variation of the AE of the Gd_2O_2S:Eu powder phosphor screens and a CsI:Tl crystal with x-ray tube voltage. Points correspond to experimental values and the solid line represents a second order polynomial fitting curve. EU: (μW s/mR m^2).

the discrepancy between Monte Carlo and the analytically calculated EAE values was higher. At low x-ray tube voltages, thick screens (139.8 mg/cm^2) absorb relatively large fractions of incident x-ray energy (e.g., $EAE_{MC}=0.51$ and $EAE_{analytical}=0.47$ at 50 kVp in Fig. 2), which is converted into light energy, and thus EAE increases. At higher voltages, x-ray photons are more penetrating and x-ray energy absorption is lower [e.g., $EAE_{MC}=0.48$ and $EAE_{analytical}=0.32$ at 80 kVp and $EAE_{MC}=0.38$ and $EAE_{analytical}=0.25$ at 130 kVp for the 139.8 mg/cm^2 screen (Fig. 2)]. The latter evaluation was made by assuming exponential x-ray absorption, governed by the screen thickness and calculated by using the x-ray mass energy absorption coefficient,[40] which expresses the amount of energy absorbed locally, i.e., at the site of interaction [see Eq. (A2) in Appendix A], while Monte Carlo predicts accurately the total energy absorbed within the whole detector mass. In our study, the discrepancy between the analytically calculated EAE and the EAE_{MC} is due to the secondary energy deposited (a) after a scattering event and (b) through fluorescence x rays after photoelectric absorption. According to Monte Carlo simulation, for the 63.1 mg/cm^2 Gd_2O_2S:Eu screen at 70 kVp, the energy absorbed through x-ray fluorescence was estimated to be 73.5%. This secondary energy is not taken into account in the analytical EAE calculation.

Figure 4 shows the variation of the AE of Gd_2O_2S:Eu screens with x-ray tube voltage in the range from 50 to 140 kVp. AE was found to increase for all screens continuously with increasing x-ray tube voltage up to 90 kVp. For higher x-ray tube voltages, AE showed a tendency to saturate (up to 110 kVp) and decrease thereafter. The thicker screen of 139.8 mg/cm^2 was found to exhibit the highest AE values at 90 kVp (20.68 EU). However, the screens of 63.1 and 78.3 mg/cm^2 were also found with high efficiency, slightly lower than that of the 139.8 mg/cm^2 screen. This finding shows that high efficiency can be also achieved with lower coating thickness which has better resolution properties as shown in Figs. 7 and 11. Table I shows AE values for various thicknesses. As it can be observed, the AE values of the screens 63.1, 78.3, and 139.8 mg/cm^2 screens are very close. An important observation from Fig. 4 is that AE maintains high values within a range of x-ray tube voltages from 40 to 140 kVp. This property is of interest for most radiographic imaging applications. Figure 4 also shows a comparison between the Gd_2O_2S:Eu and CsI:Tl scintillators. The AE of CsI:Tl (corresponding to a single crystal) was measured in a previous study[44] under experimental conditions identical to those used for the screen measurements, i.e., using a light integration sphere which assures equal light collection efficiency for both cases.[30,45] The thickness of 1 mm assigned to this CsI:Tl crystal corresponds to an estimated coating thickness of 0.451 g/cm^2. The estimated thickness was calculated by assuming a constant density of 4.51 g/cm^3, which means a packing density of 100%. Although the coating thickness of the CsI:Tl crystal is considerably higher than those of the Gd_2O_2S:Eu screens, the latter showed clearly higher AE values in the x-ray tube voltage range from 50 to 110 kVp. Thereafter, CsI:Tl shows higher AE values which, however, are very close to those of Gd_2O_2S:Eu. The DQG of the Gd_2O_2S:Eu phosphor screens is shown in Fig. 5. The shape of the DQG curves may be explained by considering the combined effects of (1) the increasing number of optical photons created per absorbed x-ray, which increases DQG with x-ray energy and correspondingly affects the variation of DQG, and (2) the x-ray absorption which, decreases with increasing tube voltages and affects DQG in a similar way. This is more evident in the high energy part of the curve. In addition, it is observed that DQG increases with increasing coating thickness. In the 50–60 kVp x-ray tube voltage range, DQG values increase up to a maximum value and decrease thereafter.

Figure 6 shows the emitted optical spectrum of Gd_2O_2S:Eu normalized to unity and the normalized spectral sensitivity distribution functions of various commonly em-

TABLE I. Variation of the AE with coating thickness (mg/cm^2) of the Gd_2O_2S:Eu powder phosphor screens at 50 and 90 kVp x-ray tube voltages.

	Phosphor screens (mg/cm^2)				
	33.1	46.4	63.1	78.3	139.8
X-ray tube voltage (kVp)	AE (μW s/mR m^2)				
50	9.034	12.798	15.810	16.061	16.563
90	11.271	15.654	20.038	20.038	20.665

ployed optical photon detectors; the actual sensitivity distributions of optical detectors cover a much wider wavelength region than the small portion of interest shown. The Gd_2O_2S:Eu spectrum contains a sharp peak at 623 nm which is in the red color region of the optical spectrum. The spectrum of Gd_2O_2S:Eu is narrow enough to assure very good spectral compatibility with the spectral sensitivities of many optical detectors. The spectra of CsI:Tl and Gd_2O_2S:Tb were obtained from a previous study.[30] Table II shows data relevant to the spectral compatibility between the optical spectra emitted by Gd_2O_2S:Eu, CsI:Tl, and Gd_2O_2S:Tb screens and the sensitivity of various optical detectors used in general (conventional or digital) radiography, such as (a) Agfa Scopix LT 2B film, (b) CCD, (c) flat panel imagers of *a*-Si:H photodiodes, and (d) CMOS sensors. For wavelengths in the range from 400 to 675 nm, the spectral compatibility was assessed by evaluating the spectral matching factor. In particular, it is observed that this factor is more significant when Gd_2O_2S:Eu screens are coupled to Agfa Scopix LT 2B (matching factor: 0.98), CCD with indium tin oxide (ITO) coating gates with microlenses (matching factor: 0.94), passivated *a*-Si:H (matching factor: 0.83), CMOS hybrid with NIR antireflection (AR) coating (matching factor: 0.98), and CMOS hybrid with blue AR coating (matching factor: 0.99). The light spectrum captured by the CCD (with infrared AR coating) is approximately 13.98% higher for Gd_2O_2S:Eu screens than for Gd_2O_2S:Tb and 15.05% higher than for the CsI:Tl phosphor. In the same manner, the light spectrum captured by the CMOS with hybrid NIR AR coating is approximately 12.25% higher for Gd_2O_2S:Eu screens than that for Gd_2O_2S:Tb and 15.31% higher from that of CsI:Tl. Almost the same matching factors values were obtained for the three scintillators with respect to flat panel imagers of passivated *a*-Si:H photodiodes.

Figure 7 shows MTF curves of Gd_2O_2S:Eu screens determined at 74 kVp (0.27 mGy). In granular phosphors, MTF is principally affected by the directivity of light generation and the light attenuation effects (scattering and absorption), e.g., the fraction of laterally directed optical photons that arrive at the screen's emissive surface. These photons spread out and cause image quality degradation. The amount of this light depends on the thickness of the screen and on the corresponding light attenuation (light absorption and light scattering) properties of the scintillator material. Thick screens (e.g., the 139.8 mg/cm^2) prepared from scintillators of low light attenuation coefficients, although exhibiting high efficiency, show lower MTF due to significant light spread effects.

Figure 8 shows a comparison of present data to MTF curves corresponding to needle-type CsI:Tl optimized for light output (HL) and image resolution (HR) (150 μm

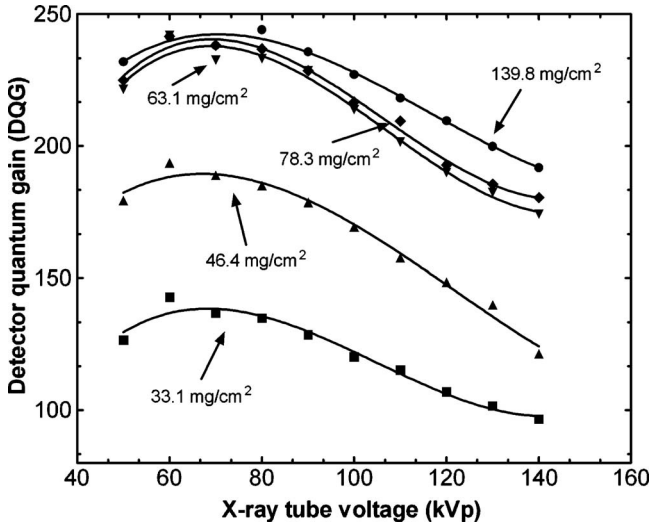

FIG. 5. Variation of DQG of Gd_2O_2S:Eu scintillators for radiography x-ray tube voltages between 40 and 140 kVp.

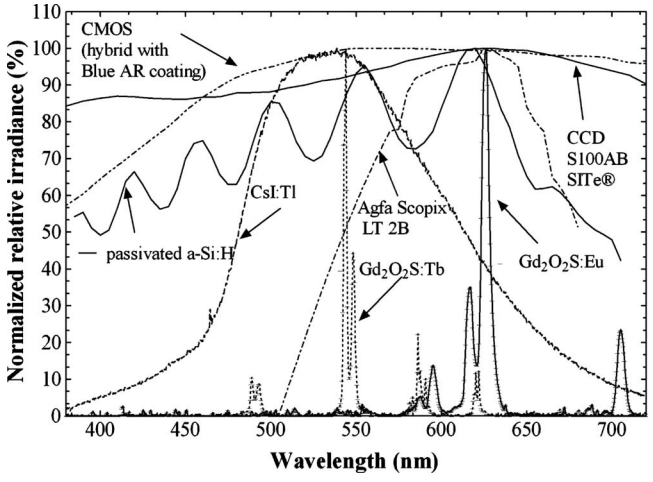

FIG. 6. Normalized emitted light spectra of Gd_2O_2S:Eu CsI:Tl and Gd_2O_2S:Tb scintillators and spectral sensitivity of various light detectors.

TABLE II. Spectral matching factors between Gd_2O_2S:Eu CsI:Tl and Gd_2O_2S:Tb phosphor materials and various optical sensors.

Optical sensors	Phosphor materials: Gd_2O_2S:Eu	CsI:Tl	Gd_2O_2S:Tb
	Spectral matching factors		
GaAsP Hamamatsu Photocathode	0.96	0.82	0.94
Agfa Scopix LT 2B	0.98	0.46	0.52
CCD S100AB SITe®[a]	0.97	0.93	0.93
CCD (IR AR coating)[a]	0.93	0.80	0.79
CCD (traditional polygates)[a]	0.84	0.66	0.60
CCD (ITO gates)[a]	0.92	0.80	0.78
CCD (ITO gates-microlenses)[a]	0.94	0.87	0.86
Passivated *a*-Si:H [b]	0.83	0.79	0.81
CMOS (hybrid NIR AR coating)[a]	0.98	0.86	0.83
CMOS (monolithic 0.25μ)[a]	0.96	0.93	0.92
CMOS (hybrid Blue AR coating)[a]	0.99	0.98	0.98
CMOS (photogate array 0.5 μm)[a]	0.92	0.86	0.79

[a]Reference 46.
[b]Reference 8.

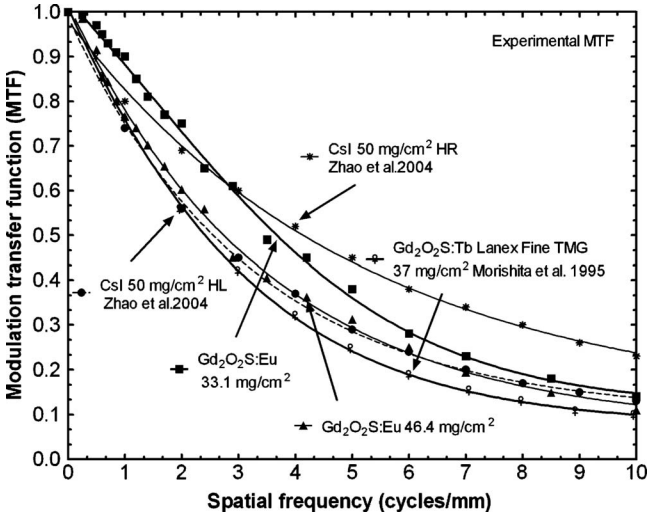

FIG. 8. MTF of the Gd_2O_2S:Eu screens determined at 74 kVp compared to CsI:Tl and Gd_2O_2S:Tb.

$\sim$50 mg/cm^2) (Ref. 47) and Gd_2O_2S:Tb scintillators,[27] published in previous studies. The 33.1 mg/cm^2 Gd_2O_2S:Eu screen was found with higher MTF than the Lanex Fine TMG screen (37 mg/cm^2 Gd_2O_2S:Tb phosphor)[27] in the whole spatial frequency range. This is probably due to the higher light extinction coefficient (m_{ext} =0.229 μm^{-1}) of Gd_2O_2S:Eu with respect to the corresponding coefficient (m_{ext}=0.218 μm^{-1}) of Gd_2O_2S:Tb as found by MC.[2] Similarly, the 46.4 mg/cm^2 Gd_2O_2S:Eu screen was found with higher MTF than that of a 50 mg/cm^2 CsI:Tl HL (Ref. 47) for spatial frequencies up to 6 mm^{-1}, but lower to a similar coating thickness CsI:Tl screen (50 mg/cm^2 HR) optimized for resolution.[47] This screen, however, has been specially processed by adding light absorbing materials between the CsI columns to minimize lateral spreading of light leading to higher MTF.

Figure 9 shows a comparison between Monte Carlo predictions and experimental MTFs. The agreement between Monte Carlo predictions and experimental MTFs was better for the 33.1 mg/cm^2 phosphor screen; for the medium to high frequency range (4–10 mm^{-1}) (agreement $\pm$2%), the model overestimated the experimental values by 2%–5%. For the 63.1 mg/cm^2 phosphor screen, higher deviations was observed in the low frequency range up to 2.9 mm^{-1} (12% difference between MC and experimental results in the 2 mm^{-1} and 19% difference in the 1 mm^{-1}). For higher spatial frequencies (3–10 mm^{-1}), MC and experimental results were in closer agreement. These deviations may be due to (a) the estimated uncertainty in experimental measurements and (b) limitations of the MC model (e.g., assumption of Poisson distribution for the production of light quanta, assumption for monochromatic light photons).

Figure 10 shows the 1D normalized noise power spectrum (NNPS) for the Gd_2O_2S:Eu screens determined at 74 kVp

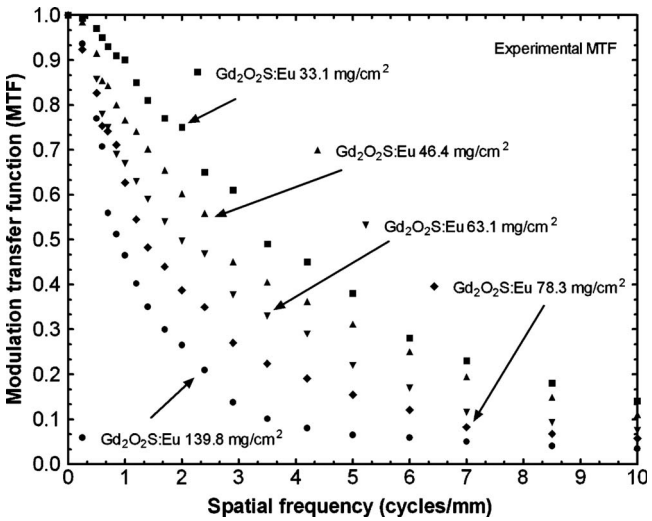

FIG. 7. MTF of the Gd_2O_2S:Eu screens determined at 74 kVp.

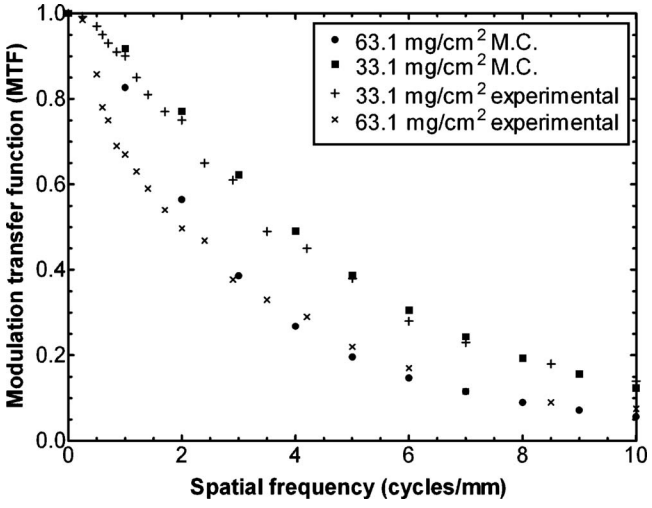

FIG. 9. MTF comparison between the experimental results and the Monte Carlo predictions for the Gd_2O_2S:Eu screens determined at 74 kVp.

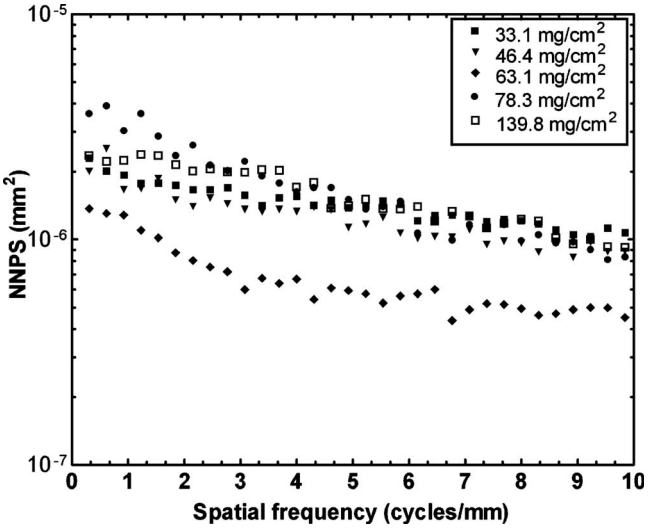

FIG. 10. NNPS for the five Gd_2O_2S:Eu screens determined at 74 kVp.

(at exposure level of 0.27 mGy equivalent to the mean exposure to the detector). The lowest NNPS was shown for the 63.1 mg/cm^2 screen. The shape of the curves are the combined effect of the image transfer characteristics of the screen, as presented in Fig. 7, and the high value of DQG, shown in Fig. 5. The 33.1 mg/cm^2 screen shows higher NNPS than the 63.1 mg/cm^2 screen due to the effect of its lower DQG [see Eq. (4) and Fig. 5].

Figure 11 shows DQE curves of various screens determined at 74 kVp (0.27 mGy). As it is observed, DQE decreased rapidly with frequency and with decreasing screen thickness. The DQE is degraded at all frequencies because of the increase in the NPS at low frequencies and the degradation of the MTF at higher frequencies. Maximum DQE was found for the screen of 139.8 mg/cm^2. In the frequency range up to 2.9 mm^{-1}, this screen maintained relatively high values ranging from 0.54 at 0.25 mm^{-1} frequency, down to 0.23 at 2.9 mm^{-1}. For spatial frequencies 3–10 mm^{-1} the

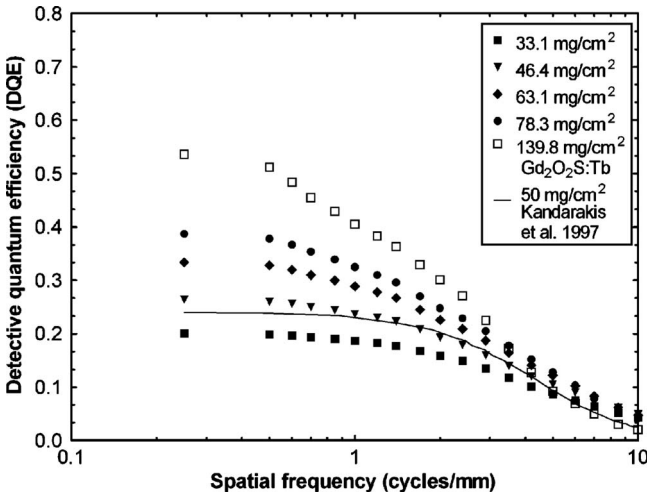

FIG. 11. DQE of various phosphor screens determined at 74 kVp (0.27 mGy).

78.3 mg/cm^{-2} thick screen progressively obtains relatively higher DQE values (up to 6 mm^{-1}) and thereafter, the 63.1 mg/cm^2 shows higher DQE. These results indicate that DQE is affected by the combined effects of the x-ray detection, MTF, noise, and efficiency behavior. DQE of the Gd_2O_2S:Eu screens was compared to previously published DQE data for Gd_2O_2S:Tb (50 mg/cm^2 determined at 90 kVp).[48] The 46.4 mg/cm^2 Gd_2O_2S:Eu screen was found with higher DQE than the 50 mg/cm^2 Gd_2O_2S:Tb for spatial frequencies up to 1.4 mm^{-1} and with approximately equal values thereafter. The values of Swank factor estimated by the MC simulation program [Eq. (8)] for the 33.1 mg/cm^2 Gd_2O_2S:Eu screen was approximately 0.6 at 74 kVp, respectively. The zero frequency DQE value [Eq. (9)] was 0.14. In all MC simulations, the relative statistical uncertainties in the predicted results did not exceed 0.1%. For the present phosphor material (Gd_2O_2S:Eu), the MTF as well as the Swank factor were predicted by using values for the m_{ext}=0.229 μm^{-1} [Eq. (6)] and g=0.759 [Eq. (7)], estimated by the MC program.[2,49]

IV. SUMMARY AND CONCLUSION

In the present study, the absolute luminescence efficiency, the modulation transfer function, and the detective quantum efficiency of Gd_2O_2:Eu powder scintillator screens were investigated. The screens were prepared in our laboratory with various thicknesses. Measurements were obtained under conditions employed in diagnostic radiology. Peak absolute efficiency was obtained for the 139.8 mg/cm^2 screen. The overall light emission efficiency of Gd_2O_2:Eu powder scintillator was found higher than that of CsI:Tl. The imaging performance of Gd_2O_2:Eu was found comparable to that of both CsI:Tl HL and Gd_2O_2:Tb. MTF of the 46.4 mg/cm^2 Gd_2O_2:Eu was found higher than a 150 μm CsI:Tl HL and the 33.1 mg/cm^2 was found higher than that of a 37 mg/cm^2 Gd_2O_2S:Tb phosphor. DQE of the 46.4 mg/cm^2 Gd_2O_2S:Eu was found higher than that of a 50 mg/cm^2 Gd_2O_2S:Tb. Taking into account the spectral compatibility of Gd_2O_2S:Eu to CMOS and Si optical sensors, this scintillator could be considered for applications in digital x-ray imaging with small framing rate.

ACKNOWLEDGMENTS

This work is funded by the Greek State Scholarships Foundation (I.K.Y.).

APPENDIX A: RADIATION DETECTION

1. Quantum detection efficiency (QDE)

The x-ray QDE for polyenergetic x-rays was calculated by Eq. (A1) (Ref. 23)

$$\mathrm{QDE} = \frac{\int_0^{E_0} \Phi_X(E)(1 - e^{-(\mu_{\mathrm{tot},t}(E)/\rho)w_0})dE}{\int_0^{E_0} \Phi_X(E)dE}. \quad \text{(A1)}$$

$\Phi_X(E)$ is the x-ray photon fluence (photons per unit of area) incident on the scintillator. $\mu_{\mathrm{tot},t}(E)/\rho$ is the x-ray total mass

attenuation coefficient of the scintillator.[40] w_0 is the screen coating thickness (mg/cm^2).

2. Energy absorption efficiency (EAE)

The EAE was calculated by Eq. (A2) (Ref. 23)

$$\mathrm{EAE} = \frac{\int_0^{E_0} \Psi_X(E)(\mu_{\mathrm{tot,en}}(E)/\mu_{\mathrm{tot},t}(E))\mathrm{QDE}(E)dE}{\int_0^{E_0} \Psi_X(E)dE}. \quad \text{(A2)}$$

$\mathrm{QDE}(E)$ is the monoenergetic quantum efficiency. $\Psi_X(E)$ is the incident x-ray energy fluence and $\mu_{\mathrm{tot,en}}(E)$ is the total mass energy absorption coefficient of the scintillator. $\mu_{\mathrm{tot,en}}(E)$ includes all mechanisms of energy deposition locally at the point of x-ray interaction within the scintillators mass. All secondary photons, e.g., *K*-characteristic fluorescence x rays, created just after the primary interaction effect, were assumed to escape the irradiated material.[23] Total attenuation $[\mu_{\mathrm{tot},t}(E)/\rho]$ and energy absorption coefficients $[\mu_{\mathrm{tot,en}}(E)]$ (cm^2/g) of the $Gd_2O_2S:Eu$, for different x-ray energies, were calculated from tabulated data on absorption and attenuation coefficients of gadolinium, sulfur, and oxygen.[40]

APPENDIX B: CONVERSION OF EXPOSURE TO FLUENCE

The x-ray fluence Φ_X required for DQG and DQE determination was estimated by converting x-ray exposure data *X* as follows:[23,50,51]

$$\Phi_X = X\hat{\Phi}, \quad \text{(B1)}$$

where $\hat{\Phi}$ is a function defined as the x-ray photon flux per exposure rate, which can be estimated as[23]

$$\hat{\Phi} = \int \Phi_X(E)dE \Big/ \left(\int \Phi_X(E)[X/\Phi_X(E)]dE \right), \quad \text{(B2)}$$

where

$$X/\Phi_X(E) = (\mu_{\mathrm{en}}(E)/\rho)_{\mathrm{air}} \cdot (W_A/e)^{-1} \cdot E \quad \text{(B3)}$$

is the factor converting photon fluence into exposure rate, $(\mu_{\mathrm{en}}/\rho)_{\mathrm{air}}$ is the x-ray mass energy absorption coefficient of air at energy *E*, and (W_A/e) is the average energy per unit of charge required to produce an electron-ion pair in air. The values of (W_A/e) and $(\mu_{\mathrm{en}}/\rho)_{\mathrm{air}}$ were obtained from the literature.[40,51]

[a]Author to whom correspondence should be addressed. Electronic mail: kandarakis@teiath.gr

[1]B. A. Arnold, in *The Physics of Medical Imaging: Recording System, Measurements and Techniques*, edited by A. G. Haus (AAPM, New York, 1979), pp. 30–37.
[2]P. Liaparinos, I. Kandarakis, D. Cavouras, H. Delis, and G. S. Panayiotakis, "Modeling granular phosphor screens by Monte Carlo methods," Med. Phys. **33**, 4502–4514 (2006).
[3]A. M. Gurvich, "Luminescent screens for mammography," Radiat. Meas. **24**, 325–330 (1995).
[4]I. Kandarakis, D. Cavouras, G. S. Panayiotakis, T. Agelis, C. D. Nomicos, and G. S. Giakoumakis, "X-ray induced luminescence and spatial resolution of $La_2O_2S:Tb$ phosphor screens," Phys. Med. Biol. **41**, 297–307 (1996).
[5]W. R. Hendee, *Medical Radiation Physics* (Year Book Medical, Chicago, 1970), pp. 145–148.
[6]M. Nikl, "Scintillation detectors for x-rays," Meas. Sci. Technol. **17**, R37–R54 (2006).
[7]P. A. Rodnyi, S. B. Mikhrin, A. N. Mishin, and A. V. Sidorenko, "Small-size pulsed x-ray source for measurements of scintillator decay time constants," IEEE Trans. Nucl. Sci. **48**, 2340–2343 (2001).
[8]J. A. Rowlands and J. Yorkston, in *Handbook of Medical Imaging: Physics and Psychophysics*, edited by J. Beutel, H. L. Kundel, and R. L. Van Metter (SPIE, Bellingham, 2000), Vol. 1, pp. 223–328.
[9]E. Zych, "Spectroscopy of Eu-activated Lu_2O_3 x-ray phosphors," in *Frontal Semiconductor Research*, edited by O. T. Chang (Nova Science, New York, 2006) pp. 1–24.
[10]V. V. Nagarkar, S. V. Tipnis, S. R. Miller, A. Lempicki, C. Brecher, P. Szupryczynski, and H. Lingertat, "A new x-ray scintillator for digital radiography," IEEE Trans. Nucl. Sci. **50**, 297–300 (2003).
[11]A. Lempicki, C. Brecher, P. Szupryczynski, H. Lingertat, V. V. Nagarkar, S. V. Tipnis, and S. R. Miller, "A new lutetia-based ceramic scintillator for x-ray imaging," Nucl. Instrum. Methods Phys. Res. A **488**, 579–590 (2002).
[12]J. M. Boone, M. Tecotzky, and G. M. Alexander, "Binary screen detector system for single-pulse dual-energy radiography," Radiology **183**, 863–870 (1992).
[13]A. Taibi, A. Del Guerra, M. Gambaccini, M. Marziani, and A. Tuffanelli, "Evaluation of a digital x-ray detector based on a phosphor-coated CCD for mammography," Nucl. Instrum. Methods Phys. Res. A **392**, 210–213 (1997).
[14]M. Gambaccini, A. Taibi, P. Baldelli, A. Del Guerra, and A. Tuffanelli, "Image noise properties of a phosphor-coated CCD x-ray detector," Nucl. Instrum. Methods Phys. Res. A **409**, 508–510 (1998).
[15]E. J. Harris, G. J. Royle, R. D. Speller, J. A. Griffiths, G. Kidane, and A. M. Hanby, "Evaluation of a novel low light level (L3 vision) CCD technology for application to diffraction enhanced breast imaging," Nucl. Instrum. Methods Phys. Res. A **513**, 27–31 (2003).
[16]M. Gambaccini, A. Taibi, A. Del Guerra, M. Marziani, and A. Tuffanelli, "MTF evaluation of a phosphor-coated CCD for x-ray imaging," Phys. Med. Biol. **41**, 2799–2806 (1996).
[17]C. Michail, I. Valais, A. Toutountzis, N. Kalyvas, G. Fountos, S. David, I. Kandarakis, and G. Panayiotakis, "Light emission efficiency of (GOS:Eu) powder screens under x-ray mammography conditions," IEEE Trans. Nucl. Sci. **55**(6), 3703–3709 (2008).
[18]S. Shigeo and M. Yen William, *Phosphor Handbook* (CRC, New York, 1998), p. 576.
[19]M. Sadowsky, "The preparation of luminescent screens," Trans. Electrochem. Soc. **95**, 112–128 (1949).
[20]G. Blasse and B. C. Grabmaier, *Luminescent Materials* (Springer, Berlin, 1994), p. 85.
[21]P. F. Liaparinos and I. S. Kandarakis, "The Monte Carlo evaluation of noise and resolution properties of granular phosphor screens," Phys. Med. Biol. **54**, 859–874 (2009).
[22]I. G. Valais, I. S. Kandarakis, D. N. Nikolopoulos, I. A. Sianoudis, N. Dimitropoulos, D. A. Cavouras, C. D. Nomicos, and G. S. Panayiotakis, "Luminescence efficiency of $Gd_2SiO_5:Ce$ scintillator under x-ray excitation," IEEE Trans. Nucl. Sci. **52**, 1830–1835 (2005).
[23]J. M. Boone, in *Handbook of Medical Imaging: Physics and Psychophysics*, edited by J. Beutel, H. L. Kundel, and R. L. Van Metter (SPIE, Bellingham, 2000), Vol. 1, pp. 36–57.
[24]J. M. Boone and A. Seibert, "An accurate method for computer generating tungsten anode x-ray spectra from 30 to 140 kV," Med. Phys. **24**, 1661–1670 (1997).
[25]I. Kandarakis, D. Cavouras, G. S. Panayiotakis, and C. D. Nomicos, "Experimental investigation of the optical signal, gain, signal-to-noise ratio and information content characteristics of x-ray phosphor screens," Appl. Phys. B: Lasers Opt. **72**, 877–883 (2001).
[26]G. T. Barnes, *The Physics of Medical Imaging: Recording System Measurements and Techniques* (AAPM, New York, 1979).
[27]J. Morishita, K. Doi, R. Bollen, P. C. Bunch, D. Hoeschen, G. Sirand-rey, and Y. Sukenobu, "Comparison of two methods for accurate measurement of modulation transfer functions of screen-film systems," Med. Phys. **22**(2), 193–200 (1995).
[28]D. Cavouras, I. Kandarakis, G. S. Panayiotakis, E. K. Evangelou, and C. D. Nomicos,"An evaluation of the $Y_2O_3:Eu^{3+}$ scintillator for application in medical x-ray detectors and image receptors," Med. Phys. **23**(12), 1965–1975 (1996).

[29]ICRU, "Modulation transfer function of screen-film systems," ICRU Report No. 41, 1986.
[30]C. Michail, G. Fountos, S. David, I. Valais, A. Toutountzis, N. Kalyvas, I. Kandarakis, and G. Panayiotakis, "A comparative investigation of $Lu_2SiO_5:Ce$ and $Gd_2O_2S:Eu$ powder scintillators for use in x-ray mammography detectors," Meas. Sci. Technol. **20**, 104008 (2009).
[31]J. C. Dainty and R. Shaw, *Image Science* (Academic, New York, 1974), pp. 232–380.
[32]M. B. Williams, P. A. Mangiafico, and P. U. Simoni, "Noise power spectra of images from digital mammography detectors," Med. Phys. **26**, 1279–1293 (1999).
[33]P. C. Bunch, K. E. Huff, and R. Van Metter, "Analysis of the detective quantum efficiency of a radiographic screen-film combination," J. Opt. Soc. Am. A **4**(5), 902–909 (1987).
[34]R. S. Holland, in *The Physics of Medical Imaging: Recording Systems, Measurements and Techniques*, edited by A. G. Haus (AAPM, New York, 1979), pp. 152–171.
[35]H. Kuhn and W. Knupfer, "Imaging characteristics of different mammographic screens," Med. Phys. **19**(2), 449–457 (1992).
[36]N. Kalivas, I. Kandarakis, D. Cavouras, L. Costaridou, C. D. Nomicos, and G. Panayiotakis, "Modeling quantum noise of phosphors used in medical x-ray imaging detectors," Nucl. Instrum. Methods Phys. Res. A **430**, 559–569 (1999).
[37]P. Monnin, D. Gutierrez, S. Bulling, D. Lepori, J. F. Valley, and F. R. Verdun, "A comparison of the performance of modern screen-film and digital mammography systems," Phys. Med. Biol. **50**, 2617–2631 (2005).
[38]R. Shaw, in *The Physics of Medical Imaging: Recording System, Measurements and Techniques*, edited by A. G. Haus (AAPM, New York, 1979), pp. 515–523.
[39]A. L. Evans, *The Evaluation of Medical Images* (Adam Hilger, Bristol, 1981), pp. 45–46.
[40]J. H. Hubbel and S. M. Seltzer, "Tables of x-ray mass attenuation coefficients and mass energy absorption coefficients 1 keV to 20 MeV for elements $Z=1$ to 92 and 48 additional substances of dosimetric interest," U.S. Department of Commerce, NISTIR Report No. 5632, 1995.
[41]E. Storm and H. Israel, "Photon cross-sections from 0.001 to 100 MeV for elements 1 through 100," Los Alamos Scientific Laboratory of the University of California, Report No. LA-3753, 1967.
[42]R. M. Nishikawa and M. J. Yaffe, "Model of the spatial-frequency-dependent detective quantum efficiency of phosphor screens," Med. Phys. **17**, 894–904 (1990).
[43]A. Ginzburg and C. E. Dick, "Image information transfer properties of x-ray intensifying screens in the energy range from 17 to 320 keV," Med. Phys. **20**(4), 1013–1021 (1993).
[44]I. Valais, D. Nikolopoulos, N. Kalivas, A. Gaitanis, G. Loudos, I. Sianoudis, N. Giokaris, D. Cavouras, N. Dimitropoulos, C. D. Nomicos, I. Kandarakis, and G. S. Panayiotakis, "A systematic study of the performance of the CsI:Tl single-crystal scintillator under x-ray excitation," Nucl. Instrum. Methods Phys. Res. A **571**, 343–345 (2007).
[45]G. Valais, "Systematic study of the light emission efficiency and the corresponding intrinsic physical characteristics of single crystal scintillators, doped with the trivalent cerium (Ce^{3+}) activator, in wide energy range (from 20 kV–18 MV) for medical applications," Ph.D. thesis, University of Patras, 2008.
[46]P. Magnan, "Detection of visible photons in CCD and CMOS: A comparative view," Nucl. Instrum. Methods Phys. Res. A **504**, 199–212 (2003).
[47]W. Zhao, G. Ristic, and J. A. Rowlands, "X-ray imaging performance of structured cesium iodide scintillators," Med. Phys. **31**(9), 2594–2605 (2004).
[48]I. Kandarakis, D. Cavouras, G. S.Panayiotakis, D. Triantis, and C. D. Nomicos, "An experimental method for the determination of spatial-frequency-dependent detective quantum efficiency (DQE) of scintillators used in x-ray imaging detectors," Nucl. Instrum. Methods Phys. Res. A **399**, 335–342 (1997).
[49]P. F. Liaparinos and I. S. Kandarakis, "The imaging performance of compact $Lu_2O_3:Eu$ powdered phosphor screens: Monte Carlo simulation for applications in mammography," Med. Phys. **36**, 1985–1997 (2009).
[50]M. B. Williams, P. U. Simoni, L. Smilowitz, M. Stanton, W. Phillips, and A. Stewart, "Analysis of the detective quantum efficiency of a developmental detector for digital mammography," Med. Phys. **26**(11), 2273–2285 (1999).
[51]J. R. Greening, *Fundamentals of Radiation Dosimetry* (Institute of Physics, London, 1985).